Chapter 9
Nanowire BioFETs: An Overview

M. Meyyappan and Jeong-Soo Lee

Abstract In this chapter, the biosensing as a key element of nanotechnology and commanding a wide range of applications is discussed, e.g., fast and efficient clinical diagnostics, health care, security, environmental monitoring, etc. The operation and sensing mechanism of BioFETs and ion-sensitive FETs are elaborated on a molecular level, based upon the molecular recognition between target and probe molecules and the input gate voltage and output ON current of the conventional FETs. In particular, the extended roles of the gate electrode of BioFETs as the probing surface are highlighted, in comparison with the conventional gate electrode, together with the physical and biological processes for detecting target molecules. Moreover, the bottom-up syntheses of vertical and horizontal nanowires are presented and the ensuing nanowires are characterized. Also, the top-down and bottom-up approaches for processing nanowires are compared by taking as criteria the process complexity and quality of the nanowires produced. Finally, the future prospects of bio-sensing are presented.

Abbreviation

LED	Light-emitting diode
UV	Ultraviolet
IR	Infrared
NEP	Noise-equivalent power
SWCNT	Single-walled carbon nanotube
FET	Field effect transistor
CVD	Chemical vapor deposition
SAED	Selected-area-electron diffraction

M. Meyyappan (✉)
NASA Ames Research Center, Moffett Field, California, USA
e-mail: m.meyyappan@nasa.gov

J.-S. Lee
Department of Electrical Engineering, Pohang University of Science and Technology, Pohang, South Korea

VLS   Vapor-liquid-solid
PECVD   Plasma enhanced chemical vapor deposition
FIB   Focused ion beam

9.1 What is the Need for Biosensing?

A biosensor is a device that can identify the presence and/or provide quantitative measurement (such as concentration) of a biochemical species in a sample. The need for biosensors is ubiquitous in modern society: clinical diagnostics, healthcare, early warning biothreat detection, water quality monitoring, food quality monitoring and related agricultural applications, environmental monitoring and many more [1–5]. The concept of a lab-on-a-chip has been around for over a couple of decades. As a system, it attempts to integrate various subsystems such as the biosensor with auxillaries including fluidic components (valves, channels etc.) to transport the samples, concentrators, separators, heaters etc. The motivation for the lab-on-a-chip is the desire to perform an entire set of analytical operations—normally done by many technicians in a laboratory—just at the chip level. The advantages are obvious: speed (minutes to an hour vs. days), smaller sample volumes, and cost savings through automation. These systems are developed typically on silicon, glass or plastic substrates and designed to be disposable, at least in the area of biomedical and clinical diagnostic applications. For example, routine health screening may need a system that can monitor pH, cholesterol, complete blood count, white blood cell count, urine analysis, biomarkers for heart disease, and the metabolic panel (Na, K, Ca, etc.). Municipal water quality monitoring typically involves analysis for about fifteen pathogens including E-coli, salmonella, and other bacteria, protozoa and viruses.

9.2 Biosensors

The sensor is the critical component of the system discussed above and may typically work based on a "lock and key" approach. Alternatively known as the affinity-based approach, it involves choosing a probe *a priori* that is designed to bind selectively to the target of interest [1]. The probe can be of any type including DNA, RNA, antibody, aptamer and others. The binding event manifests as a change in some measurable property of the surface supporting it. For example, a cantilever may show different bending levels for the bare cantilever, after functionalization with the probe, and following the probe-target hybridization. Optical techniques include monitoring the fluorescence or surface plasmon resonance. One of the most common methods is to measure current or voltage from an electrode. Aside from

electrochemical measurements [2, 4, 6–10] involving cyclovoltammetry, amperometry and impedance spectroscopy, electrical transduction also includes monitoring the change in current–voltage characteristics of a field effect transistor (FET) appropriately treated with the biological probes [5, 11–24]. Fabrication and characterization of semiconducting nanowire-based biological FET or BioFET and its applications are the subject of this chapter.

9.3 What is a BioFET?

The biofield effect transistor is a special form of FET used for sensing biomolecules in a fluid system (see Fig. 9.1). The conventional field effect transistor is a three-terminal device consisting of source, gate, and drain electrodes. The gate regulates the current flow between the source and the drain just like a valve regulates fluid flow due to the pressure difference between two points in a pipe. The analogous driving force in the FET is the voltage difference between the source and the drain. The FET is a unipolar device, implying that current is conducted only by electrons or holes.

The essential part of a BioFET—also known as ion sensitive FET or ISFET—is the gate electrode replaced by the gate dielectric, electrolyte, and a reference electrode [25–30]. The electrical contact to the electrolyte is provided by a reference electrode which is placed in the electrolyte solution. The channel conductance or resistance is modulated by the electrostatic field generated by the reference electrode. Usually, the channel is covered by dielectric materials such as Al_2O_3, Si_3N_4, SiO_2, Ta_2O_5 [30]. The ion concentration in the electrolyte affects the electrostatic field and the channel potential across the electrolyte/dielectric/semiconductor system.

In pH-sensing applications, the H^+-specific binding sites on the surface can be protonated and deprotonated, and thus, a variation of pH value will change the

Fig. 9.1 Schematic of a BioFET
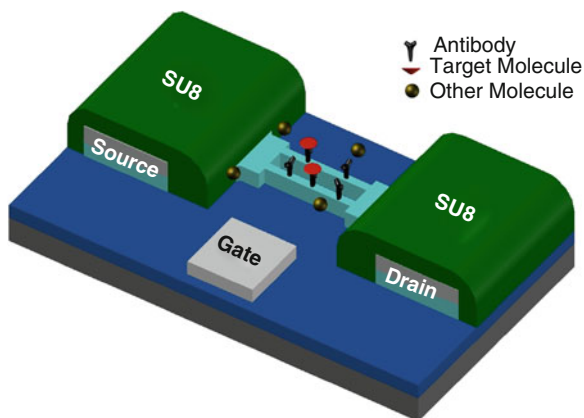
channel potential. For example, the hydroxyl group at the surface can exchange protons with the electrolyte via the following chemical reactions.

$$SiOH \Leftrightarrow SiO^- + H^+$$

$$SiOH + H^+ \Leftrightarrow SiOH_2^+$$
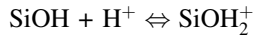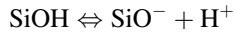
The typical binding sites are the hydroxyl groups on the oxide surface and the silanol (SiH_3OH) and amine ($SiNH_2$) groups on the nitride surface.

In biosensing applications, a probe molecule, which is immobilized on the dielectric surface, binds selectively with the target molecule in the electrolyte. This binding event can change the channel potential and then be detected by measuring the change of drain current or gate voltage.

9.4 Nanowire Synthesis

For the construction of nanowire-based BioFETs, a choice must be made first about the material, and then, an appropriate synthesis technique for that nanowire needs to be selected. From a conventional manufacturing point-of-view and future integration with processing chips, silicon nanowire appears to be the safe choice. Nevertheless, a variety of other materials, particularly oxide nanowires such as In_2O_3, ZnO etc., have been pursued in the literature. Regardless of the material, the nanowires can be fabricated either by a bottom-up approach or conventional top-down method involving etching to produce the desired cylindrical nanowire form out of a thin or thick film. Both approaches are described below. A detailed background on inorganic nanowires, growth methods, properties and applications including biosensors can be found in Ref. [31].

9.4.1 Bottom-Up Synthesis Techniques

The material choices for nanowires are Si, Ge, metal oxides etc. as mentioned earlier and these materials have long been grown as thin and thick films using chemical vapor deposition (CVD) and other epitaxial techniques. In the bottom-up preparation of nanowires also, the same precursors or source gases are used at more or less the same processing conditions as in the case of thin film growth. Then, what makes nanowire growth possible? There must be a guiding force to form the cylindrically shaped nanowires. An obvious choice would be to use a preformed template with the desirable pore size that can guide the growth into cylindrical nanowires. Anodized alumina is the most commonly used template for this purpose, and a wide variety of nanowires have been successfully grown using this template. The disadvantage of this method is that the template itself needs to

be removed prior to the use of the nanowires in device fabrication. Often the template removal is achieved through some acid treatment which may damage the nanowire and/or introduce defects.

A successful alternative to template growth is a catalyzed-CVD approach, often known as the vapor-liquid-solid (VLS) technique [31]. A laboratory VLS reactor is a quartz tube inserted into a two-zone furnace shown in Fig. 9.2. The source vapor can be generated in any number of ways in the upstream zone depending on the desired material, as will be discussed shortly. The growth substrate consists of a catalyst, typically a thin metal layer (gold, In, Ga etc.) or mono-dispersed colloids of that metal, if readily available. The catalyst layer may be prepared either by sputtering or thermal evaporation. At the growth temperature, this thin layer breaks up into tiny droplets which remain in a molten state. The source vapor dissolves into the droplet and when supersaturation is reached, material begins to precipitate in the form of nanowires as shown in Fig. 9.3. Invariably, the catalyst particle ends up at the top of the growing nanowire in the VLS process which allows easy removal through acid wash or chemical mechanical polishing of vertical nanowires during device processing.

In the case of silicon nanowires, silane (or $SiCl_4$) diluted in H_2 may be used as feedstock as in the case of the corresponding thin film growth [31–34]. For GaAs nanowires, $(CH_3)_3Ga/AsH_3$ feedstock common in MOCVD may be used [31, 35, 36]. For most oxide nanowires, the common practice in VLS growth is sublimation of the corresponding high purity (99.999 % or higher) powder [31, 37, 38]. This sublimation approach also works well for a variety of tellurides, selenides and other materials as long as the high purity powder form of the source is available [39–42] and the sublimation temperature is reasonable without the need for high temperature furnaces (over 1,000 °C). It is possible to mix two or more source powders for growing ternary nanowires [43] (e.g., $Ge_2Sb_2Te_5$). Gold is the widely used catalyst in nanowire growth reported in the literature. Gold modulates carrier recombination in both n- and p-type silicon, since high-mobility interstitial gold atoms can transform into electrically active substitutional sites. Therefore, it is desirable to look for alternatives to gold. Fortunately, a wide variety of group III, IV, V, and VI metal elements have been found to be useful as catalyst except for Ir and Pt [44]. The only correlation appears to be the inverse dependence of nanowire growth density on the melting point of the catalyst metal. In this regard, indium (In) is a low-melting metal that is useful as a catalyst for the growth of Si and other nanowires, allowing growth zone temperature to be as low as 150 °C [45]. Gallium also is another low-melting candidate ($\sim$450 °C) suitable for nanowire growth [46].

Figure 9.4 shows a random mat of silicon nanowires grown on a silicon substrate [32]. The diameter of the nanowire correlates reasonably with the catalyst particle diameter. The length of the nanowires is several microns which can be decreased by reducing the growth time. Figure 9.5 shows vertically oriented silicon nanowires grown using a mixture of $SiCl_4/H_2$ with diameter in the range of 40–80 nm and height 1–2 μm. Only a very narrow set of conditions using this feedgas system yield vertical nanowires in the case of silicon [32]. For example,
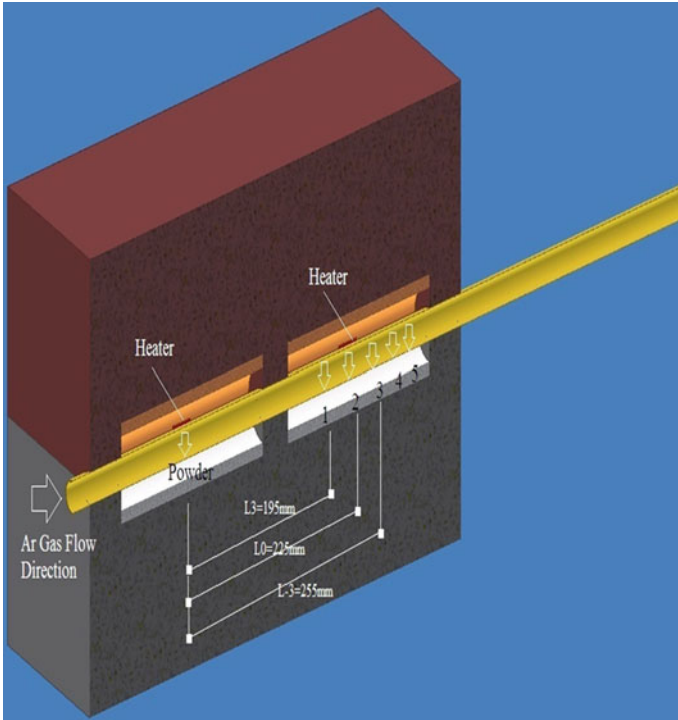
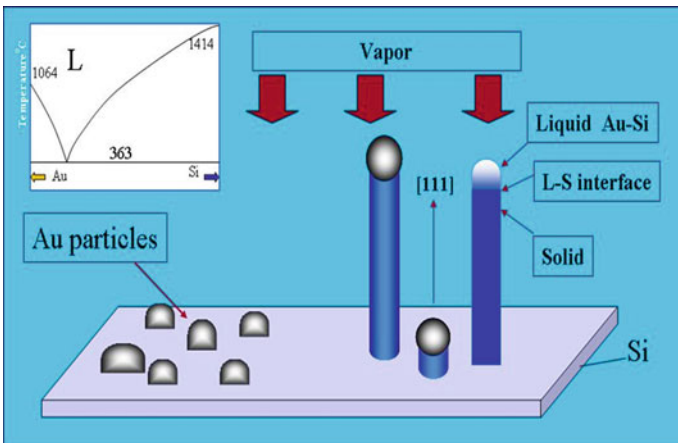**Fig. 9.2** Reactor for nanowire growth by VLS approach (figure courtesy of Keivan Davami)

Fig. 9.3 VLS growth mechanism (figure courtesy of Xuhui Sun)

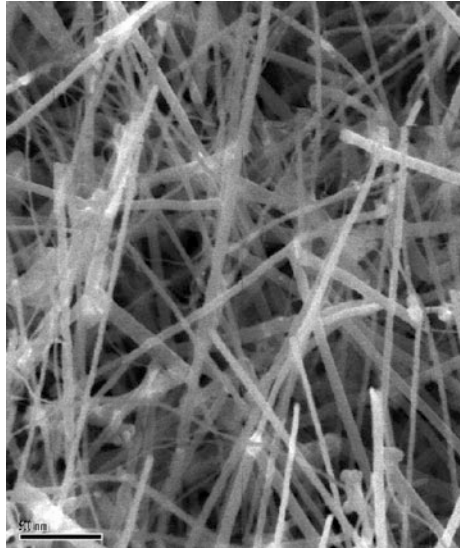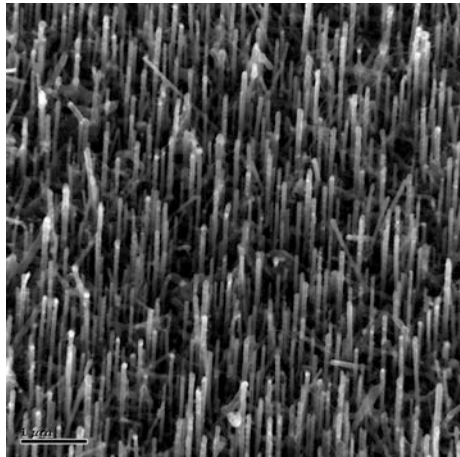**Fig. 9.4** Random mat of silicon nanowires grown by VLS method (figure courtesy of Aaron Mao)

Fig. 9.5 Vertical silicon nanowires grown by VLS approach (figure courtesy of Aaron Mao)

$SiCl_4$ fractions greater than 0.25 % in H_2 and temperatures greater than 950 °C yield thin and curvy wires. Similarly, a narrow set of conditions have been identified for growing vertical silicon nanowires using the silane/H_2 system as well [33]. The silicon nanowires can be doped with boron and phosphorous to obtain p- and n-type, respectively, as in the case of thin films [31].

The as-grown nanowires typically show exceptional surface quality, ideal for device fabrication. It has been shown for a variety of different semiconductor nanowires that the bandgap increases with a decrease in diameter, particularly for sizes below the value of the corresponding Bohr radius. For example, a silicon nanowire of 1.3 nm in diameter exhibits a bandgap of 3.5 eV, substantially larger

than the 1.1 eV for bulk silicon [47]. This allows bandgap engineering through control of the nanowire diameter. In spite of all the attractive features of the bottom-up technique, it is hard to use these structures in device fabrication in a straightforward manner. For example, attempting a "pick and place" approach using the random mat of nanowires seen in Fig. 9.4 over thousands of pairs of source-drain terminals on a large wafer is a difficult task. Direct growth by catalyzed-CVD (i.e. VLS) on the prefabricated contacts for thousands of devices over a large wafer is not easy either. The vertical nanowires can be used to fabricate vertical surround gate transistors. In this configuration, the source will be at the bottom with the drain contact at the top; the gate wraps around the nanowire channel connecting the source and the drain. The report on such devices using SiNWs uses many nanowires under one gate [48]. A gate surrounding only a single nanowire was reported for ZnO transistor [49]. In any case, wafer-scale fabrication of vertical nanowire transistors has not been achieved yet.

9.4.2 Top-Down Nanowires

Fabrication of nanowires using a top-down approach is straightforward with the use of patterned etching to obtain nanowires of desired diameter and length. Figure 9.6 shows an array of silicon nanowires created using dry etching [50]. Control of the nanowire diameter and length as well as the number of nanowires in the channel region is much easier compared with the bottom-up process discussed above. This is the major advantage of the top-down approach in addition to the immediate possibility of large wafer (200–300 mm) fabrication.

9.5 Device Fabrication and Performance

In recent years, a number of reports on the fabrication and performance of nanowire based BioFETs have appeared including a variety of bottom-up grown nanowires [51–64] and a few conventional top-down efforts [24, 50, 65–67]. Below a concise summary of these works is presented.

Fig. 9.6 Silicon nanowires prepared by a top-down process involving patterning followed by dry etching (figure courtesy of Taiuk Rim and Sungho Kim)
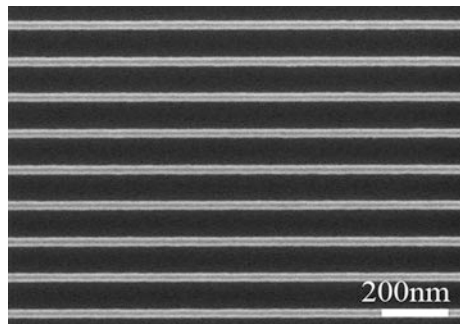
9.5.1 BioFETS Using Bottom-Up Grown Nanowires

Cui et al. [52] were one of the first to report nanowire-based devices for biosensing. They prepared silicon nanowires using a VLS approach, aligned them using a flow approach and contacted two ends of a nanowire with electron-beam lithography. The back-gated device was the first NW-BioFET to show a pH-dependent conductance. The SiNWs were also modified with biotin for the detection of streptavidin down to picomolar concentration levels. This group also demonstrated the utility of NW-BioFETs for sensitive detection of cancer markers [55]. Incorporation of surface receptors into arrays of NWs allowed selective detection of mucin-1, carcinoembryonic antigen, and prostate-specific antigen (PSA). A comprehensive analysis of their device characteristics showed that the NW-BioFETs provide the highest conductance response in the subthreshold regime along with the best charge detection limit [54].

Though silicon is the most common nanowire used in biosensor construction, oxide nanowires have been explored as well. In_2O_3 nanowires have been found to possess good conductance for NW-FET construction [56–59]. Li et al. fabricated back-gated FETs using VLS-grown In_2O_3 nanowires with a channel length of 2 μm. They attached PSA antibodies to the nanowire surface and demonstrated a sensitivity of 5 ng/mL of PSA using a single nanowire conducting channel. This group also used antibody mimic proteins which are 2–5 nm polypeptides showing strong binding capability to their targets just like antibodies to detect nucleocapsid protein [59]. The latter is a biomarker for severe acute respiratory syndrome (SARS). The In_2O_3 NW-FET using nanowires modified with a fibronectin-based binding apent detected N-protein at subnanomolar concentrations. This sensitivity is comparable to many immunological detection techniques, but the NW-FET provides results in a shorter time without the need for labeling.

Another metal oxide popular for biosensing is ZnO and the nanowire form provides a stable oxide surface and a high surface-to-volume ratio. Choi et al. [60] grew ZnO nanowires by pulsed laser deposition, which are 70 nm in diameter and about 8 μm long. The nanowires functionalized with biotin were sensitive to streptavidin binding and the device was able to detect 2.5 nM of streptavidin. Yeh et al. [61] used a ZnO nanowire device and showed that a nonsymmetrical Schottky contact under reverse bias is much more sensitive than a device with symmetric ohmic contacts. Single nanowire ZnO FET has been shown to detect uric acid as low as 1 pM concentration with a 14.7 nS conductance increase [62].

Finally, it is of interest to know the effects of nanowire diameter, number of nanowires (single vs. multiple) etc. on sensitivity and other BioFET metrics. Li et al. [63] conducted an investigation of these effects using silicon nanowire FETs. They found that the sensitivity decreased with an increase in nanowires, increase in nanowire diameter, and higher doping density. For example, devices with 4 and 7 nanowires showed 38 and 82 % lower sensitivity than nanowires 61–80 nm in diameter. An increase in doping density from 10^{17} to 10^{19} cm^{-3} results in a 69 % decrease in sensitivity.
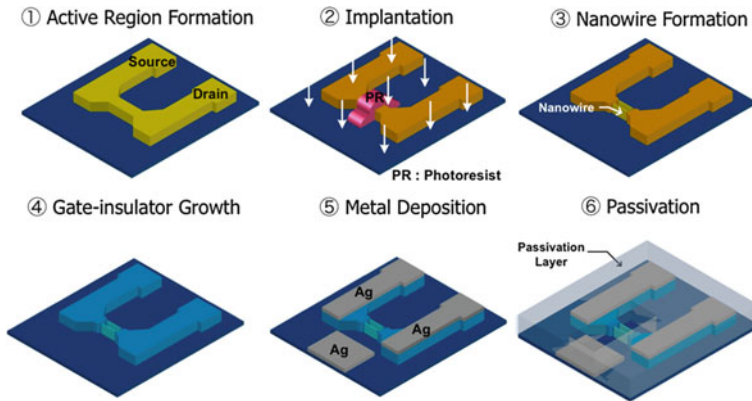
Fig. 9.7 Top-down process sequence for the fabrication of silicon nanowire ISFET (figure courtesy of Taiuk Rim and Sungho Kim)

9.5.2 Top-Down BioFETs

A schematic diagram of the SiNW ISFET fabrication process is shown in Fig. 9.7 along with a schematic of the device in Fig. 9.8. A 6-inch silicon-on-insulator (SOI) substrate with 10^{15} cm^{-3} boron doping was used. The 675-μm-thick substrate consists of 100-nm thick <100> oriented silicon layer and a 200-nm-thick buried oxide layer. The top Si layer was thinned to 40 nm using thermal oxidation at 900 °C and wet etching of SiO$_2$ with diluted HF (1:1,000 with deionized water) to form the rectangular-shaped nanowires. The top Si layer, except the active region, was etched using an inductively coupled plasma reactive ion etcher (ICP-RIE) with a mixture of HBr and O$_2$. After the device isolation process, nanowires of 50-nm width and 10 micron length were formed using electron-beam
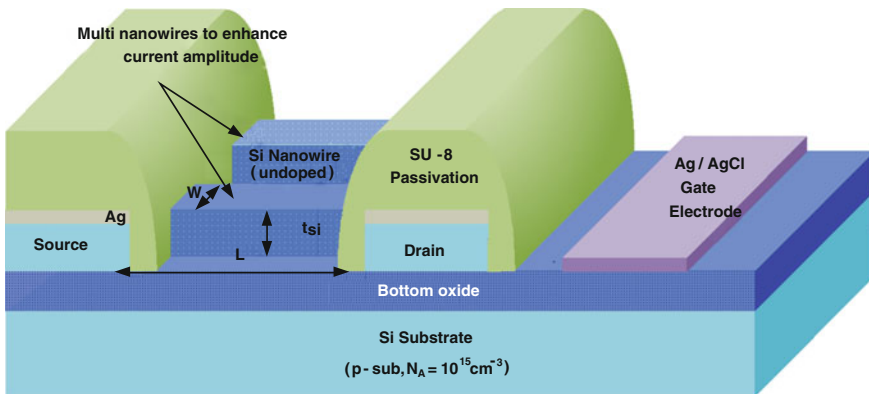

Fig. 9.8 Schematic of a Si-NW ISFET (figure courtesy of Taiuk Rim and Sungho Kim)

lithography and ICP-RIE. A 4-nm thick SiO_2 sacrificial oxide layer was grown using thermal oxidation at 900 °C to protect the interface between the nanowire channel and gate oxide from the ion implant damage. Arsenic ion implantation was then done to form the source and drain ohmic contacts, and the implanted dopants were activated using rapid thermal annealing at 1,000 °C for 25 s. The damaged sacrificial oxide was removed next by immersing in diluted HF solution and a 5-nm thick gate oxide was grown in a thermal furnace at 900 °C. The source/drain contact pads and the gate electrodes (20-nm-thick Ti and 200-nm-thick Ag layers) were deposited using an electron-beam evaporator and patterned using conventional lithography and a lift-off process. Finally, the surface of the entire device, except for the active sensing region and the contact pads, was covered with a 2-mm-thick SU-8 layer to prevent leakage current between the contacts and the solution. The width, length, and height of the well holding the solution over the devices were 1,200, 1,200, and 2 μm, respectively. For the formation of integrated Ag/AgCl pseudo reference electrode, 30 μL of 0.1 M KCl was dropped on top of the embedded Ag electrode and a voltage of 1 V was applied for 300 s. Due to the reaction between silver and chloride ions, the Ag/AgCl pseudo reference electrode (RE) was successfully fabricated for use as a gate electrode of the SiNW ISFET. The width and length of the Ag/AgCl reference electrode were 1,000 and 1,000 μm, respectively.

Figure 9.9 shows the drain current (I_D) versus gate voltage (V_G) characteristics of the above SiNW ISFET with the drain voltage (V_D) varied between 0.1 and 0.7 V. The results indicate successful modulation of the channel conductance by the embedded Ag/AgCl gate electrode. During the measurement, the gate voltage was swept from 0 to 1.5 V at a rate of 50 mV/s and the source and substrate voltages were set to ground. The SiNW ISFET shows typical n-type FET behavior with a high on–off ratio of 10^5 and a good subthreshold-slope of 100-mV/dec. Inspection of transfer curves of the SiNW ISFET under different pH conditions (not shown here) shows a lateral shift of the curves without degradation of the

Fig. 9.9 Current-voltage characteristics of SiNW ISFET shown in Fig. 9.8 (figure courtesy of Taiuk Rim and Sungho Kim)
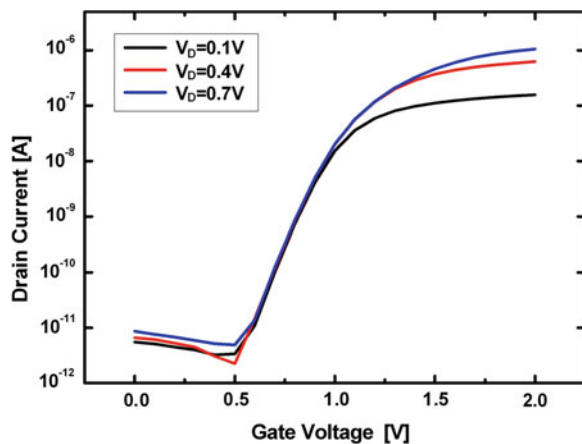
on-current and the sub-threshold slope. The V_{TH} of the device is found to increase linearly as the pH value increases. The total threshold voltage shift is 400 mV, and the pH sensitivity of the SiNW ISFET device is 40 mV/pH, which is a typical value for ISFETs using SiO_2 gate insulator as a sensing layer.

Stern et al. [24] also fabricated SiNW-FETs using a top-down approach and demonstrated a sensitivity of less than 10 fM specific label-free antibody detection. Tian et al. [66] fabricated a multinanowire FET and showed pH sensing with a linear response over a range of 2–9. Their NW-FET was also able to do selective detection of bovine serum albumin at concentrations of 0.1 fM.

9.6 Summary, Challenges, and Future Outlook

Biofield effect transistors (BioFETs) have been emerging as a viable candidate for biosensor systems for a wide variety of applications in health care, security, environmental monitoring etc. Silicon has been the typical material of choice for the conducting channel although other materials, such as metal oxides, have also been considered. Nanostructures for enhanced sensitivity have been explored with carbon nanotubes and graphene as leading candidates. In this chapter, a detailed account on the use of silicon nanowires in BioFETs has been presented. Both bottom-up and top-down approaches for the preparation of SiNWs have been discussed. The device fabrication details differ significantly between the two methods. The constraint today on the bottom-up SiNW synthesis techniques includes the lack of amenability for wafer scale fabrication. It is not possible to precisely grow nanowires (of chosen diameter and length) between each pair of source and drain over a 200 or 300 mm wafer. "Pick and place" approaches from bulk samples are unlikely to lead to large scale production either. As of now, there have been no credible routes to large scale device fabrication using bottom-up techniques.

In contrast, the top-down approach is readily adaptable for wafer-scale fabrication. Control of length and diameter of the nanowires is also relatively easier. Therefore, this approach seems to be a more promising route, at least for now. Regardless of the approach or material of choice, the development to date has been limited to the working of the sensor, that is, probe attachment, hybridization, and signal transduction. Fully functional systems require integration of microfluidics (channels, valves etc.) on the same chip. Microfluidics is a well evolved field, especially on silicon platforms. Therefore, integration of the sensor, signal processing, and microfluidics for sample handling along with system packaging should not pose serious challenges.

Whether it is clinical diagnostics or any other applications mentioned earlier, the early use of the sensor systems may be in the laboratory setting where the labor hours on analytical tests can be drastically reduced. From then on, migration into field use is expected to follow; this can include at-home diagnostics of viruses and infectious diseases or routine health checkup functions, municipal water quality

monitoring at designated sites, pollution monitoring in rivers and lakes etc. The platforms for such field-use are likely to be different from those in the laboratory or a central lab. In this regard, smart phones may play an important role in hosting the biosensor systems. Currently, smart phone–based gas/vapor and biosensors are being investigated in many academic and industrial laboratories across the world. It is entirely possible to integrate into a smart phone a chip consisting of an array of BioFETs, or equivalent devices, along with microfluidics capabilities with the goal of performing multiplexed operations. In a health-related application, disposal cartridges will have to be employed necessarily. Even the design of microfluidics in a smart phone environment may not be challenging. The true challenge is to eliminate the need for concentrating or purifying or any other type of time-consuming sample processing, and still delivering reliable and sensitive diagnostics.

References

1. Daniels, J. S., & Pourmand, N. (2007). Label-free impedance biosensors: opportunities and challenges. *Electroanal, 19*, 1239–1257.
2. Grieshaber, D., Mackenzie, R., Voros, J., & Reimhult, E. (2008). Electrochemical biosensors—sensor principles and architecture. *Sensors, 8*, 1450–1458.
3. Cosnier, S., & Mailley, P. (2008). Recent advances in DNA sensors. *Analyst, 133*, 984–991.
4. Gooding, J. J. (2002). Electrochemical DNA hybridization sensors. *Electroanal, 14*, 1145–1156.
5. Lee, C. S., Kim, S. K., & Kim, M. (2009). Ion-sensitive field-effect transistor for biological sensing. *Sensors, 9*, 7111–7131.
6. Ronkainen, N. J., Halsall, H. B., & Heineman, W. R. (2010). Electrochemical biosensors. *Chemical Society Reviews, 39*, 1747–1763.
7. Wei, D., Bailey, M. J. A., Andrew, P., & Ryhanen, T. (2009). Electrochemical biosensors at the nanoscale. *Lab on a Chip, 9*, 2123–2131.
8. Monosik, R., Stred'ansky, M., Sturdik, E. (2012). Application of electrochemical biosensors in clinical diagnostics. *Journal of Clinical Laboratory Analysis*, *26*, 22–34.
9. Yogeswaran, U., & Chen, S. M. (2008). A review on the electrochemical sensors and biosensors composed of nanowires as sensing material. *Sensors, 8*, 290–313.
10. Li, J. (2004).Biosensors. In M. Meyyappan (Ed.), *Carbon nanotubes: science and applications.* Boca Raton: CRC Press.
11. Ingerbrandt, S., & Offerhausser, A. (2006). Label-free detection of DNA using field-effect transistors. *Physica Status Solidi (a), 203*, 3395–3411.
12. Schafer, S., Eick, S., Hofmann, B., Dufaux, T., Stockmann, R., Wrobel, G., et al. (2009). Time-dependent observation of individual cellular binding events to field-effect transistors. *Biosensors & Bioelectronics, 24*, 1201–1208.
13. Poghossian, A., Ingebrandt, S., Offenhausser, A., & Schoning, M. J. (2009). Field-effect devices for detecting cellular signals. *Seminars in Cell & Developmental Biology, 20*, 41–48.
14. Sakata, T., & Miyahara, Y. (2007). Direct transduction of allele-specific former extension into electrical signal using generic field effect transistor. *Biosensors & Bioelectronics, 22*, 1311–1316.

15. Sohn, Y. S., & Kim, Y. T. (2008). Field-effect transistor type C-reactive protein sensor using cysteine-tagged protein G. *Electronics Letters, 44*, 955–956.
16. Park, K. M., Lee, S. K., Sohn, Y. S., & Choi, S. Y. (2008). BioFET sensor for detection of albumin in urine. *Electronics Letters, 44*, 185–186.
17. Park, K. Y., Sohn, Y. S., Kim, C. K., Kim, H. S., Bae, Y. S., & Choi, S. Y. (2008). Development of a FET-type albumin sensor for diagnosing nephritis. *Biosensors & Bioelectronics, 23*, 1904–1907.
18. Eteshola, E., Keener, M. T., Elias, M., Shapiro, J., Brillson, L. J., Bhushan, B., et al. (2008). Engineering functional protein interfaces for immunologically modified field effect transistor (ImmunoFET) by molecular genetic means. *Journal of the Royal Society Interface, 5*, 123–127.
19. Gupta, S., Elas, M., Wen, X., Shapiro, J., Brillson, L., Lu, W., et al. (2008). Detection of chemically relevant levels of protein analyte under physiologic buffer using planar field effect transistors. *Biosensors & Bioelectronics, 24*, 505–511.
20. Hsiao, C. Y., Lin, C. H., Hung, C. H., Su, C. J., Lo, Y. R., Lee, C. C., et al. (2009). Novel poly-silicon nanowire field effect transistors for biosensing application. *Biosensors & Bioelectronics, 24*, 1223–1229.
21. Lin, C. H., Hsiao, C. Y., Hung, C. H., Lo, Y. R., Lee, C. C., Su, C. J., et al. (2008). Ultrasensitive detection of dopamine using a polysilicon nanowire field effect transistor. *Chemical Communications, 44*, 5749–5751.
22. Freeman, R., Elbaz, J., Gill, R., Zayats, M., & Willner, I. (2007). Analysis of dopamine and tyrosinase activity on ion-sensitive field-effect transistor (ISFET) devices. *Chemistry—A European Journal, 13*, 7288–7293.
23. Zayats, M., Huang, Y., Gill, R., Ma, C. A., & Willner, I. (2006). Label-free and reagentless aptamer-based sensors for small molecules. *Journal of the American Chemical Society, 128*, 13666–13667.
24. Stern, E., Klemic, J. F., Routenberg, D. A., Wyrembak, P. N., Turner-Evans, D. B., Hamilton, A. D., et al. (2007). Label-free immunodetection with CMOS-compatible semiconducting nanowires. *Nature, 445*, 519–522.
25. Bergveld, P. (1970). Development of an ion sensitive solid state device for neurophysiological measurements. *IEEE Transactions on Biomedical Engineering, 17*, 70–71.
26. Caras, S., & Janata, J. (1980). Field effect transistor sensitive to penicillin. *Analytical Chemistry, 52*, 1935–1937.
27. Schoning, M., & Poghossian, A. (2006). BioFEDs (field effect devices): state of the art and new directions. *Electroanal, 18*, 1893–1900.
28. Bergveld, P. (2003). Thirty years of ISFETOLOGY—what happened in the past 30 years and what may happen in the next 30 years. *Sensors and Actuators, 13*(88), 1–20.
29. Schoning, M., & Poghossian, A. (2002). Recent advances in biologically sensitive field effect transistors (BioFETs). *Analyst, 127*, 1137–1151.
30. Yuqing, M., Jianguo, G., & Jianrong, C. (2003). Ion sensitive field effect transducer-based biosensors. *Biotechnology Advances, 21*, 527–534.
31. Meyyappan, M., & Sunkara, M. K. (2010). *Inorganic nanowires: applications, properties and characterization*. Boca Raton: CRC Press.
32. Mao, A., Ng, H. T., Nguyen, P., McNeil, M., & Meyyappan, M. (2005). Silicon nanowire synthesis by a vapor-liquid-solid approach. *Journal of Nanoscience and Nanotechnology, 5*, 31–835.
33. Westwater, J., Gosain, D. P., Tomiya, S., Usui, S., & Ruda, H. (1997). Growth of silicon nanowires via gold/silane vapor-liquid-solid reaction. *Journal of Vacuum Science & Technology, 13*(15), 554–557.
34. Aella, P., Ingole, S., Potuskey, W. T., & Picraux, T. (2007). Influence of plasma stimulation on Si nanowire nucleation and orientation control. *Advanced Materials, 19*, 2603–2607.
35. Johansson, J., Wacaser, B. A., Kick, K. A., & Seifert, W. (2006). Growth related aspects of epitaxial nanowires. *Nanotechnology, 17*, 5355–5361.

36. Noborisaka, J., Motohisa, J., & Fukui, T. (2005). Catalyst-free growth of GaAs nanowires by selective-area metalorganic vapor-phase epitaxy. *Applied Physics Letters, 86*, 21302.

37. Nguyen, P., Ng, H. T., Kong, J., Cassell, A. M., Quinn, R., Li, J., et al. (2003). Epitaxial directional growth of indium-doped tin oxide nanowire arrays. *Nano Letters, 3*, 925–928.

38. Nguyen, P., Vaddiraju, S., & Meyyappan, M. (2006). Indium and tin oxide nanowires by vapor-liquid-solid growth technique. *Journal of Electronic Materials, 35*, 200–206.

39. Sun, X. H., Yu, B., Ng, G., Nguyen, T.D., Meyyappan, M. (2006). III–V compound semiconductor indium selenide (In₂Se₃) nanowires: synthesis and characterization. *Applied Physics Letters*, *89*, 233121.

40. Davami, K., Kang, D., Lee, J. S., & Meyyappan, M. (2011). Synthesis of ZnTe nanostructures by vapor-liquid-solid technique. *Chemical Physics Letters, 504*, 62–66.

41. Davami, K. H., Ghassemi, M., Sun, X. H., Yassar, R. S., Lee, J. S., Meyyappan, M. (2011). *In situ* observation of morphological change in CdTe nano- and submicron wires. *Nanotechnology*, *22*, 35204.

42. Sun, X., Yu, B., Ng, G., & Meyyappan, M. (2007). One dimensional phase charge nanostructures: Germanium telluride nanowire. *Journal of Physical Chemistry C, 11*, 2421–2425.

43. Sun, X., Yu, B., & Meyyappan, M. (2007). Synthesis and nanoscale thermal encoding of phase charge nanowires. *Applied Physics Letters, 90*, 183116.

44. Nguyen, P., Ng, H. T., & Meyyappan, M. (2005). Catalyst metal selection for the synthesis of inorganic nanowires. *Advanced Materials, 17*, 1773–1777.

45. Sun, X., Calebotta, G., Yu, B., Seluaduray, G., & Meyyappan, M. (2007). Synthesis of germanium nanowires on insulator catalyzed by indium or antimony. *Journal of Vacuum Science & Technology, 13*(25), 415–420.

46. Sunkara, M. K., Sharma, S., Miranda, R., Lian, G., & Dickey, E. C. (2001). Bulk synthesis of silicon nanowires using a low temperature vapor-liquid-solid method. *Applied Physics Letters, 79*, 1546–1548.

47. Ma, D. D. D., Lee, C. S., Au, F. C. K., Tong, S. Y., & Lee, S. T. (2003). Small-diameter silicon nanowire surfaces. *Science, 299*, 1874–1877.

48. Schmidt, V., Riel, H., Snez, S., Karg, S., Riess, W., & Gosele, U. (2006). Realization of a silicon nanowire vertical surround-gate field-effect transistor. *Small, 2*, 85–88.

49. Ng, H. T., Han, J., Yamada, T., Nguyen, P., Chen, P., & Meyyappan, M. (2004). Single crystal nanowire vertical surround-gate field effect transistor. *Nano Letters, 4*, 1247–1252.

50. Kim, S., Rim, T., Lee, U., Baek, E. H., Lee, H., Baek, C. H., et al. (2011). Silicon nanowire ion sensitive field effect transistor with integrated Ag/AgCl electrode: pH sensing and noise characteristics. *Analyst, 136*, 5012–5016.

51. Timko, B. P., Karni-Cohen, T., Quan, Q., Bozhi, T., & Lieber, C. M. (2010). Design and implementation of functional nanoelectric interfaces with biomolecules, cells and tissues using nanowire device arrays. *IEEE Transactions on Nanotechnology, 9*, 269–280.

52. Cui, Y., Wei, Q., Park, H., & Lieber, C. M. (2001). Nanowire nanosensors for highly sensitive and selective detection of biological and chemical species. *Science, 293*, 1289–1292.

53. Patolsky, F., Zheng, G., & Liber, C. M. (2006). Nanowire-based biosensors. *Analytical Chemistry, 78*, 4260–4269.

54. Gao, X. P. A., Zheng, G., & Lieber, C. M. (2010). Subthreshold regime has the optimal sensitivity for nanowire FET sensors. *Nano Letters, 10*, 547.

55. Zheng, G., Patolsky, F., Cui, Y., Wang, W. U., & Lieber, C. M. (2005). Multiplexed electrical detection of cancer markers with nanowire sensor arrays. *Nature Biotechnology, 23*, 1294–1301.

56. Curreli, M., Li, C., Sun, Y., Lei, B., Gunderson, M., Thompson, M. E., et al. (2005). Selective functionalization of In₂O₃ nanowire mat devices for biosensing application. *Journal of the American Chemical Society, 127*, 6922–6923.

57. Curreli, M., Zhang, R., Ishikawa, F. N., Chang, K. K., Cote, R. J., Zhou, C., et al. (2008). Real-time, label-free detection of biological entities using nanowire-based FETs. *IEEE Transactions on Nanotechnology, 7*, 651–667.

58. Li, C., Curreli, M., Lin, H., Lei, B., Ishikawa, F. N., Datar, R., et al. (2005). Complimentary detection of prostate specific antigen using In_2O_3 nanowires and carbon nanotubes. *Journal of the American Chemical Society, 127*, 12484–12485.
59. Ishikawa, F. N., Chang, H. K., Curreli, M., Liao, H., Olson, A. C., Chen, P. C., et al. (2009). Label-free electrical detection of the SARS virus N-protein with nanowire biosensors utilizing antibody mimics as capture probes. *ACS Nano, 3*, 1219–1224.
60. Choi, A., Kim, K., Jung, H. I., & Lee, S. Y. (2010). ZnO nanowire biosensors for detection of biomolecular interation in enhancement mode. *Sensors and Actuators, 13*(148), 577–582.
61. Yeh, P. H., Li, Z. L., & Wang, Z. L. (2009). Schottky-gated probe-free ZnO nanowire biosensor. *Advanced Materials, 21*, 4975–4978.
62. Liu, X., Lin, P., Yan, X., Kars, Z., Zhao, Y., Lei, Y., Li, C., Du, H., Zhang, Y. (2012). Enzyme-coated single ZnO nanowire FET biosensor for detection of uric acid. *Sensors and Actuators 13*.
63. Li, J., Zhang, Y., To, S., You, L., & Sun, Y. (2011). Effect of nanowire number, diameter and doping density on nano-FET biosensor sensitivity. *ACS Nano, 5*, 6661–6668.
64. Liu, Y. C., Rieben, N., Iversen, L., Sorensen, B. C., Park, J. W., Nygard, J., et al. (2010). Specific and reversible immobilization of histidine-tagged proteins on functionalized silicon nanowires. *Nanotechnology, 21*, 245105.
65. Vu, X. I., Stockmenn, R., Wolfrum, B., Offenhausser, A., & Ingebrandt, S. (2010). Fabrication and application of microfluidic embedded silicon nanowire biochip. *Physica Status Solidi A, 207*, 850–857.
66. Tian, R., Regonda, S., Gao, J., Liu, Y., & Hu, W. (2011). Ultrasensitive protein detection using lithographically defined Si multi-nanowire field effect-transistor. *Lab on a Chip, 11*, 1952–1962.
67. Duan, X., Li, Y., Rajan, N. K., Routenberg, D. A., Modis, Y., & Reed, M. A. (2012). Quantification of the affinities and kinetics of protein interactions using silicon nanowire biosensors. *Nature Nanotechnology, 7*, 401–407.